Enhancing the photocurrent and photoluminescence of single crystal monolayer MoS$_2$ with resonant plasmonic nanoshells

Ali Sobhani,[1,a)] Adam Lauchner,[2,a)] Sina Najmaei,[3,a)] Ciceron Ayala-Orozco,[4] Fangfang Wen,[4] Jun Lou,[3] and Naomi J. Halas[1,2,b)]

[1]*Department of Electrical and Computer Engineering, Rice University, Houston, Texas 77005, USA*
[2]*Department of Physics and Astronomy, Rice University, Houston, Texas 77005, USA*
[3]*Department of Materials Science and NanoEngineering, Rice University, Houston, Texas 77005, USA*
[4]*Department of Chemistry, Rice University, Houston, Texas 77005, USA*

Monolayer molybdenum disulfide (MoS$_2$) produced by controlled vapor-phase synthesis is a commercially promising new two-dimensional material for optoelectronics because of its direct bandgap and broad absorption in the visible and ultraviolet regimes. By tuning plasmonic core-shell nanoparticles to the direct bandgap of monolayer MoS$_2$ and depositing them sparsely (<1% coverage) onto the material's surface, we observe a threefold increase in photocurrent and a doubling of photoluminescence signal for both excitonic transitions, amplifying but not altering the intrinsic spectral response. © 2014 AIP Publishing LLC. [http://dx.doi.org/10.1063/1.4862745]

The realization of graphene growth by chemical synthesis has led to significant commercial interest in the employment of graphene's unique optoelectronic properties arising from its two-dimensional (2D) nature.[1–3] Advances in chemical synthesis have recently been made for several 2D materials, including hexagonal boron nitride,[4] germanium sulfide,[5] and molybdenum disulfide (MoS$_2$),[6–9] enabling a scalable path toward commercial applications of their distinctive properties. MoS$_2$, a semiconducting transition metal dichalcogenide, is of particular interest due to the emergence of a direct bandgap as it approaches monolayer thickness.[10–14] Recently, several groups have demonstrated photodetection from mechanically exfoliated single layer MoS$_2$[15,16] and multilayer MoS$_2$ sheets.[17,18] Single layer MoS$_2$ has been shown to possess a direct bandgap of 1.8 eV (in contrast to the 1.2 eV indirect bandgap of bulk MoS$_2$).[7,19] As a result of this direct bandgap, monolayer MoS$_2$ is a more efficient light-absorber (per layer) than its bulk phase,[7] however, its subnanometer thickness results in a low absorption cross section.

Absorption enhancement can be achieved by utilizing the strong local field concentration of plasmons, coherent oscillations of free electrons in metallic nanostructures at optical frequencies, at the resonant wavelength of the nanostructure. Consequently, several groups have demonstrated the role of plasmonics in enhancing the measured photocurrent from both prototypical semiconducting materials[20] and 2D materials.[21,22] In this manuscript we resolve the theoretically predicted excitonic transitions from the absorption peaks in the wavelength-sensitive photovoltaic signal of monolayer MoS$_2$ and we demonstrate the enhancement of these peaks in both photocurrent and photoluminescence (PL) spectra by tuning the plasmonic resonance of

silica-gold nanoshells (AuNS) to the energy region of the excitonic transitions in monolayer MoS$_2$.

Chemical vapor deposition (CVD)-grown MoS$_2$ monolayers were synthesized following the recipe as previously reported in which we expose MoO$_3$ to sulfur at high temperature and allow for the growth of MoS$_2$ single crystals.[6] Large single-crystal monolayers (SCM) of MoS$_2$ were initially identified using optical microscopy, then characterized by Raman spectroscopy to confirm their monolayer nature. The mobility of the SCM MoS$_2$ is in the range of 2–10 cm^2/(V s), measured with Hall effect probes. The uniform continuous growth of SCM MoS$_2$ results in the macroscopic triangular shaped crystals as shown in Figure 1(a). Electrodes were patterned on top of triangular individual crystals using photolithography and then backgated to form a photosensitive Field Effect Transistor (photoFET) device. The scanning electron micrograph and schematic of a typical photoFET are shown in Figures 1(a) and 1(b), respectively.

To enhance the intrinsically low absorption cross section of monolayer MoS$_2$, we exploit the tunable plasmon resonance of AuNS. Resonant light is absorbed efficiently by the AuNS, generating a local field at the surface of the MoS$_2$. This results in enhanced electron-hole pair generation in the monolayer and an increased photocurrent.[23,24] We have deposited AuNS on the device surface with an average interparticle distance of less than 1 μm to avoid plasmon coupling between adjacent nanoparticles, typically at a surface concentration of <1% (varying from 0.2% to 0.6%). The scattering cross section of AuNS on the MoS$_2$ monolayer is measured with darkfield spectroscopy under unpolarized white light illumination, showing a strong scattering maximum in the spectral region of 600–700 nm (Figure 2(a)). The AuNS were designed to have a SiO$_2$ core with a 60 nm radius and an outer Au shell thickness of 30 nm.

The plasmonic enhancement of both the photocurrent spectrum and the photoluminescence spectrum was observed. We clearly observe an enhancement (Figure 2(b), green spectrum) of more than a factor of three in the photocurrent responsivity, while the spectral shape remains

---

[a)]A. Sobhani, A. Lauchner, and S. Najmaei have contributed equally to this work.
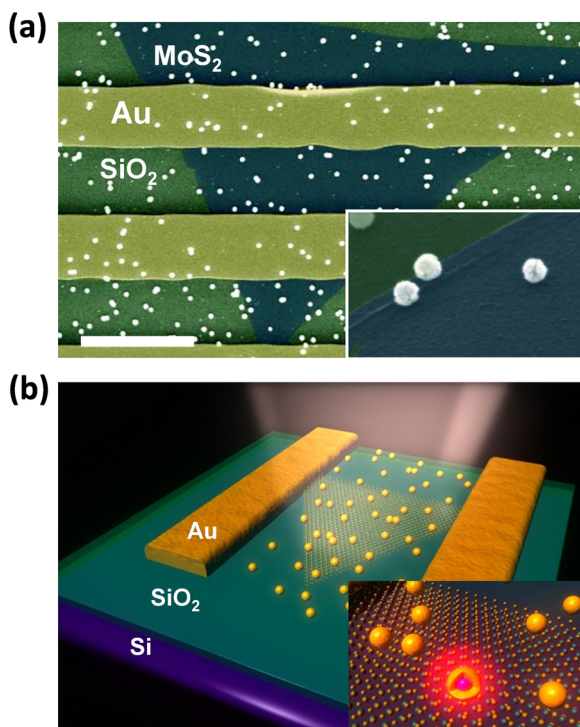[b)]Author to whom correspondence should be addressed. Electronic mail: halas@rice.edu.

(a)

(b)

FIG. 1. (a) Scanning electron micrograph of MoS$_2$ device coated with nanoshells. Monolayer MoS$_2$ is the blue triangle underneath the yellow gold electrodes. The scale bar is 5 μm. The inset is a higher magnification image of nanoshells on the surface. (b) Schematic of the MoS$_2$ phototransistor. The inset represents a magnified view of nanoshells on MoS$_2$.

consistent with that of the pristine device (Figure 2(b), red spectrum). Enhancement factors ranged between 1.5 and 3.5 across multiple tested devices due to experimental variations in the dispersion of AuNS atop the MoS$_2$, implying that enhancement could be more dramatically increased with optimization of the AuNS surface coverage.

For PL spectroscopy, the device is excited with a 514 nm laser before and after coverage with the dispersed AuNS (Fig. 2(c)). Placing AuNS on the MoS$_2$ surface and again measuring the PL with the same laser at equal laser power, we detect a PL signal which is approximately twice that of

the pristine sample. The higher PL signal is likely the direct result of increased photoabsorption in the MoS$_2$ due to the AuNS (Figure 2(c), green curve). PL spectroscopy confirms the improvement seen in the photocurrent signal (Figure 2(b)) after placing AuNS on the surface.

The photocurrent responsivity of pristine MoS$_2$ photoFET (Figure 2(b), red curve) displays two peaks, one at 630 nm (1.97 eV) and the other at 680 nm (1.82 eV). These peaks are in good agreement with the calculated direct-gap excitonic transitions for a single layer MoS$_2$.[10,25] The two peaks in the spectral signature arise from spin-orbit coupling of the valance band electrons at the K symmetry point of the direct bandgap.[10,26,27] The energy difference of the band separation is 150 meV, in agreement with literature values.[28] The sharp decay in the photocurrent spectra at wavelengths longer than 680 nm indicates the absence of the indirect bandgap in the monolayer. This is qualitatively distinct from the absorption spectra of bulk MoS$_2$, where the indirect bandgap of 1.3 eV causes an additional shoulder in the spectrum at nominally 960 nm in wavelength.[17] Similarly, PL of pristine MoS$_2$ (Figure 2(c), red curve) shows two peaks, one at ~630 nm (1.97 eV) and the other at ~682 nm (1.81 eV). The locations of these peaks are very close to the peak positions measured with photocurrent spectroscopy. The relative strength of these two peaks is also in good agreement with the expectations for single-layer MoS$_2$, where the PL signal of the higher energy transition (~2 eV) is seen to decay to nearly zero as the number of layers decreases.[7,10] For both photocurrent and photoluminescence, the addition of AuNS serves only to increase the overall signal level and has very little effect on the position of the detected peaks.

To demonstrate that the measured photocurrent is being produced solely within the MoS$_2$, we spatially mapped the responsivity of the device (Figure 3). Laser illumination of 645 nm, 680 nm, and 750 nm was used to map the photocurrent. The laser spot was focused to ~2 μm in diameter and the beam spot was rastered over the device area with no significant change in the laser beam intensity. The left-most image in Figure 3 shows the scanning electron micrograph of the laser-scanned area; the current was measured between
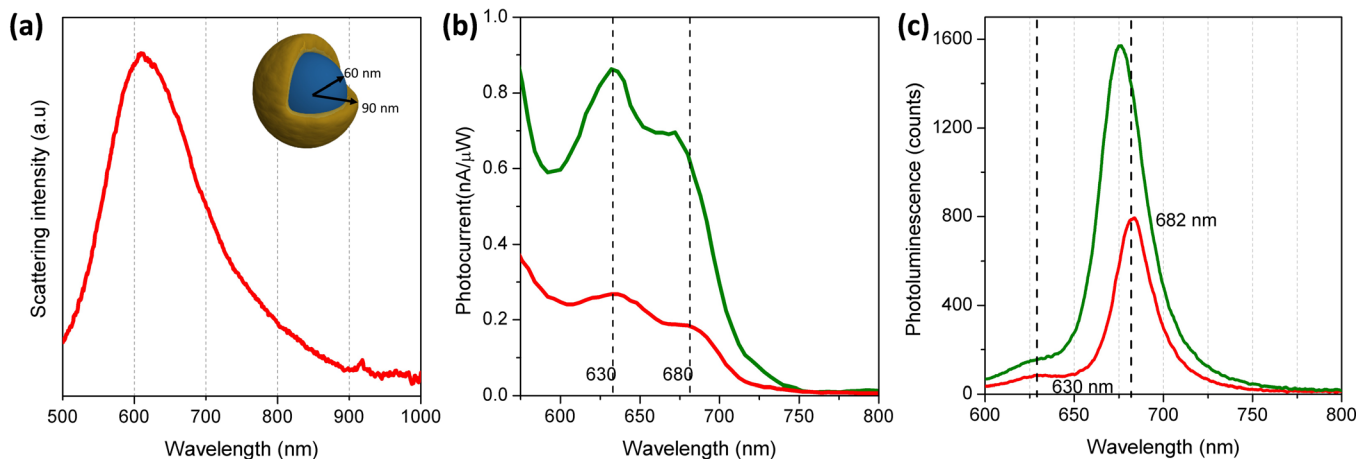
(a)

(b)

(c)

FIG. 2. (a) The scattering spectrum of gold nanoshells deposited on top of the MoS$_2$ monolayer on 300 nm silica measured with darkfield spectroscopy under unpolarized white light illumination. The nanoshell dimensions are indicated on the inset graphic. (b) Photocurrent spectroscopy on MoS$_2$ monolayer before (red curve) and after (green curve) dispersing gold nanoshells on the MoS$_2$. Two photocurrent peaks are seen in pristine MoS$_2$ at 630 nm and 680 nm. (c) Photoluminescence spectra of monolayer MoS$_2$ on silica with (green) and without (red) gold nanoshells. For pristine monolayer MoS$_2$, photoluminescence presents peaks at 630 nm and 682 nm.
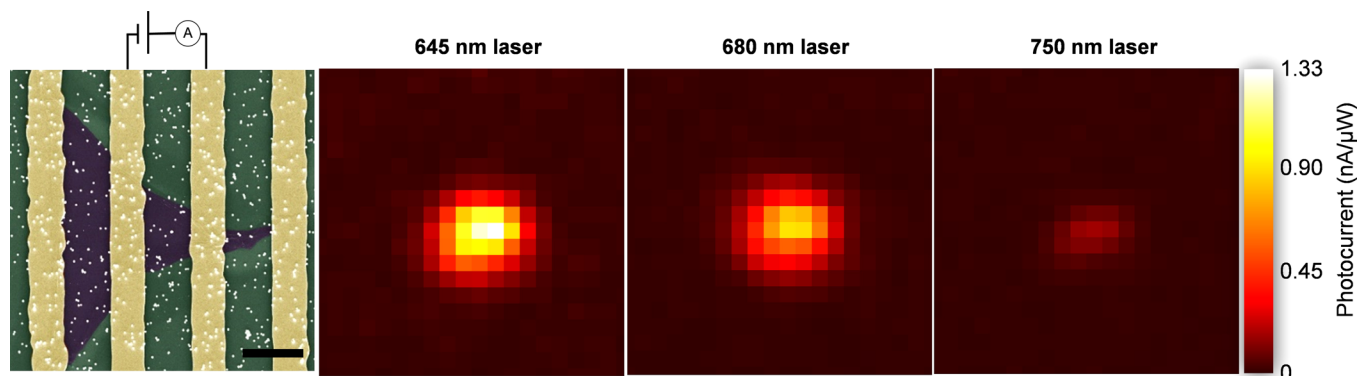
FIG. 3. (Left-most image) Scanning electron micrograph of gold electrodes and gold nanoshells on top of a MoS_2 showing the physical laser scan area for the three plots to its right; the scale bar is 5 μm. A source-drain voltage of 1 V is applied across the middle electrodes and a gate voltage of 80 V is applied via back gate; the photocurrent is measured across the middle electrodes as illustrated by the circuit. Three different laser wavelengths 645 nm, 680 nm, and 750 nm (from left to right) are used to raster the device spatially and map the photocurrent.

the two middle electrodes as indicated by the illustration of the circuit. A reduction in the photocurrent signal as the laser wavelength was varied from 645 nm to 680 nm to 750 nm is consistent with the spectral shape of the photocurrent in Figure 2(b). Figure 3 establishes that all the photocurrent measured between the electrodes comes from the excited carriers in MoS_2 and no additional signal appears to be obtained from either gold electrodes or the substrate. As a further validation of the photocurrent properties, we have observed that the photocurrent signal remains stable with repeated laser on/off cycles and that its response time is less than 6 ms for both on and off laser switching.

In summary, we have investigated CVD-grown MoS_2 single crystals using photocurrent spectroscopy. The measured photocurrent reveals two distinct absorption peaks, confirmed with our photoluminescence spectra, at 1.82 eV and 1.97 eV which are in good agreement with theoretical predictions for the direct excitonic transitions in MoS_2. We show that the absorption can be enhanced by more than a factor of three with less than 1% surface concentration of plasmonic silica-gold nanoshells tuned to the region of excitonic transition. This plasmonic enhancement is observed in both photocurrent and photoluminescence signals without altering the intrinsic spectral features. The observation that single-crystal MoS_2 properties are strongly enhanced by bandgap-resonant plasmonic nanoparticles, even at very low concentrations, paves the way toward the coupling of plasmonic nanoparticles and nanostructures to this unique 2D layered direct-gap semiconductor for further modification of its electronic and optical properties.

Photocurrent spectroscopy was performed by illumination with an ultrabroadband-supercontinuum laser (Fianium SC400) with wavelength selection from an Acousto-Optical Tuning Filter. The laser beam was focused to $\sim$2 μm in diameter; small enough to place the laser spot in the center of a 4 μm gap between the electrodes to avoid contact effects. Photocurrent responsivities were acquired using a lock-in amplifier (Signal Recovery 780) referenced to the 1.3 kHz modulated laser beam. Phase-sensitive measurement is important to avoid the convolution of thermal effects in our measurements of MoS_2 caused by the laser beam. All photocurrent measurements performed here were done under 80 V gate voltage and 1 V source-drain voltage.

PhotoFET fabrication is done by growing SCM MoS_2 on a SiO_2 (300 nm on Si wafer) substrate and employing a single step ultraviolet lithography for patterning the electrodes on top of MoS_2. For lithography, we spun-coated LOR8A as a lift-off resist for 40 s and 3500 RPM, then the sample was soft baked for 4 min at 160 °C. We did the same spin coating process on S1813 photoresist and baked it for 1 min at 110 °C. After mask alignment and ultraviolet exposure, we developed our sample in MF-319 for 45 s. 4/100 nm of Ti/Au was evaporated on the sample and it was soaked in PG Remover (to dissolve LOR8A) and Acetone (to dissolve S1813) repeatedly. LOR8A is used to improve the lift off and to avoid sonication (which alters contacts destructively). After fabrication, the samples were annealed at 200 °C for 90 min in a furnace purged with hydrogen and nitrogen to improve the electrode contact resistance and to improve the material's visible absorbance. Prior to the measurements, to further reduce surface contamination, we put the samples in 4×10^{-8} Torr vacuum for more than 6 h to remove contamination from the MoS_2 and the contacts.

For dispersing the AuNS on the photodetector surface, the device was treated with a 1% solution of poly4-vinylpyridine (PVP) to create a homogenous adhesion on the device surface. After functionalizing the device surface with PVP, we put a droplet of AuNS suspended in water solution on the MoS_2 devices and waited for 10 min before rinsing with de-ionized water and blowing with dry nitrogen. This method has been shown to provide a clean and uniform particle dispersion on the substrate[29] without negatively impacting the plasmonic resonance or the charge transfer from the AuNS.[30] The existence of PVP on the sample is crucial; without a homogenous adhesion layer the particles will tend to aggregate which broadens, red-shifts, and decreases the amplitude of the plasmonic resonance.[31,32]

[1]T. Mueller, F. Xia, and P. Avouris, Nat. Photonics **4**(5), 297–301 (2010).

[2]J.-H. Chen, C. Jang, S. Xiao, M. Ishigami, and M. S. Fuhrer, Nat. Nanotechnol. **3**(4), 206–209 (2008).

[3]F. J. Nelson, V. K. Kamineni, T. Zhang, E. S. Comfort, J. U. Lee, and A. C. Diebold, Appl. Phys. Lett. **97**(25), 253110 (2010).

[4]K. K. Kim, A. Hsu, X. Jia, S. M. Kim, Y. Shi, M. Hofmann, D. Nezich, J. F. Rodriguez-Nieva, M. Dresselhaus, T. Palacios, and J. Kong, Nano Lett. **12**(1), 161–166 (2012).

[5]C. Li, L. Huang, G. P. Snigdha, Y. Yu, and L. Cao, ACS Nano **6**(10), 8868–8877 (2012).

[6]S. Najmaei, Z. Liu, W. Zhou, X. Zou, G. Shi, S. Lei, B. I. Yakobson, J.-C. Idrobo, P. M. Ajayan, and J. Lou, Nature Mater. **12**(8), 754–759 (2013).

[7]G. Eda, H. Yamaguchi, D. Voiry, T. Fujita, M. Chen, and M. Chhowalla, Nano Lett. **11**(12), 5111–5116 (2011).

[8]K.-K. Liu, W. Zhang, Y.-H. Lee, Y.-C. Lin, M.-T. Chang, C.-Y. Su, C.-S. Chang, H. Li, Y. Shi, H. Zhang, C.-S. Lai, and L.-J. Li, Nano Lett. **12**(3), 1538–1544 (2012).

[9]Y. Zhan, Z. Liu, S. Najmaei, P. M. Ajayan, and J. Lou, Small **8**(7), 966–971 (2012).

[10]K. F. Mak, C. Lee, J. Hone, J. Shan, and T. F. Heinz, Phys. Rev. Lett. **105**(13), 136805 (2010).

[11]A. Splendiani, L. Sun, Y. Zhang, T. Li, J. Kim, C.-Y. Chim, G. Galli, and F. Wang, Nano Lett. **10**(4), 1271–1275 (2010).

[12]G. Eda and S. A. Maier, ACS Nano **7**(7), 5660–5665 (2013).

[13]X. Huang, Z. Zeng, and H. Zhang, Chem. Soc. Rev. **42**(5), 1934–1946 (2013).

[14]M. Chhowalla, H. S. Shin, G. Eda, L.-J. Li, K. P. Loh, and H. Zhang, Nature Chem. **5**(4), 263–275 (2013).

[15]Z. Yin, H. Li, H. Li, L. Jiang, Y. Shi, Y. Sun, G. Lu, Q. Zhang, X. Chen, and H. Zhang, ACS Nano **6**(1), 74–80 (2012).

[16]B. Radisavljevic, A. Radenovic, J. Brivio, V. Giacometti, and A. Kis, Nat. Nanotechnol. **6**(3), 147–150 (2011).

[17]W. Choi, M. Y. Cho, A. Konar, J. H. Lee, G.-B. Cha, S. C. Hong, S. Kim, J. Kim, D. Jena, J. Joo, and S. Kim, Adv. Mater. **24**(43), 5832–5836 (2012).

[18]H. S. Lee, S.-W. Min, Y.-G. Chang, M. K. Park, T. Nam, H. Kim, J. H. Kim, S. Ryu, and S. Im, Nano Lett. **12**(7), 3695–3700 (2012).

[19]K. K. Kam and B. A. Parkinson, J. Phys. Chem. **86**(4), 463–467 (1982).

[20]S. H. Lim, W. Mar, P. Matheu, D. Derkacs, and E. T. Yu, J. Appl. Phys. **101**(10), 104309 (2007).

[21]T. J. Echtermeyer, L. Britnell, P. K. Jasnos, A. Lombardo, R. V. Gorbachev, A. N. Grigorenko, A. K. Geim, A. C. Ferrari, and K. S. Novoselov, Nat. Commun. **2**, 458 (2011).

[22]J. Lin, H. Li, H. Zhang, and W. Chen, Appl. Phys. Lett. **102**(20), 203109 (2013).

[23]D. M. Schaadt, B. Feng, and E. T. Yu, Appl. Phys. Lett. **86**(6), 063106 (2005).

[24]S. P. Sundararajan, N. K. Grady, N. Mirin, and N. J. Halas, Nano Lett. **8**(2), 624–630 (2008).

[25]R. Coehoorn, C. Haas, J. Dijkstra, C. J. F. Flipse, R. A. de Groot, and A. Wold, Phys. Rev. B **35**(12), 6195–6202 (1987).

[26]T. Li and G. Galli, J. Phys. Chem. C **111**(44), 16192–16196 (2007).

[27]L. F. Mattheiss, Phys. Rev. B **8**(8), 3719–3740 (1973).

[28]K. F. Mak, K. He, C. Lee, G. H. Lee, J. Hone, T. F. Heinz, and J. Shan, Nature Mater. **12**(3), 207–211 (2013).

[29]B. E. Brinson, J. B. Lassiter, C. S. Levin, R. Bardhan, N. Mirin, and N. J. Halas, Langmuir **24**(24), 14166–14171 (2008).

[30]Q. Xu, F. Liu, W. Meng, and Y. Huang, Opt. Express **20**(S6), A898–A907 (2012).

[31]M. Quinten, Appl. Phys. B **73**(4), 317–326 (2001).

[32]L. Hirsch, A. Gobin, A. Lowery, F. Tam, R. Drezek, N. Halas, and J. West, Annu. Biomed. Eng. **34**(1), 15–22 (2006).